CRACK IDENTIFICATION IN MULTIPLE CRACKED BEAMS MADE OF FUNCTIONALLY GRADED MATERIAL BY USING STATIONARY WAVELET TRANSFORM OF MODE SHAPES

Tran Van Lien[1,*]**, Ngo Trong Duc**[2]
[1]*National University of Civil Engineering, Hanoi, Vietnam*
[2]*Design Consultant and Investment of Construction, Ministry of Defense, Hanoi, Vietnam*
*E-mail: lientv@nuce.edu.vn

Abstract. This paper presents crack identification in multiple cracked beams made of functionally graded material (FGM) by using stationary wavelet transform (SWT) of mode shapes and taking into account influence of Gaussian noise. Mode shapes are obtained from multiple cracked FGM beam element and spring model of cracks. The theoretical development was illustrated and validated by numerical examples. The investigated results show that crack identification method by using SWT of mode shapes is efficient and realizable.

Keywords: crack identification; multiple cracked beam; functionally graded material (FGM); stationary wavelet transform (SWT); mode shapes.

1. INTRODUCTION

Functionally graded material (FGM) have been proved to be an advanced material by its advantaged properties compared to the laminate composites and by the wide application in the high-tech industries such as aerospace, automobile, electronics, optics, chemistry, biomedical engineering etc. Because presence of a crack in a structure usually leads to reduction of stiffness and change the dynamic characteristics, the crack problem in FGM is greatly important to evaluate structure's serviceability and integrity. The most important result of the fracture mechanics for FGM [1–3] is that a crack in FGM beam can be modeled by an equivalent massless spring of stiffness calculated from the crack depth.

Determination of dynamic characteristics of cracked FGM beam can be obtained by using analytical [3–11], Galerkin's semi-analytical [12], finite element method (FEM) and dynamic stiffness method (DSM). The FEM has been developed and employed for modal analysis and identification of FGM beams [13–16]. As the FEM is formulated on the base of frequency independent polynomial shape function, it could not be used to capture all necessary high frequencies and mode shapes of interest. An alternative approach called DSM fulfilled the gap of FEM by using frequency-dependent shape functions that are

found as exact solution of vibration problem in the frequency domain [17–21]. Although exact solutions of the vibration problem are not easily constructed for complete structures, but they, if were available, enable to study exact response of the beam in arbitrary frequency range.

The problem of crack identification in FGM structures gets also increasing attention of either structural engineers or researchers. A lot of procedures have been emerged to detect and quantify cracks in structures. Banerjee et al. [15] proposed two different two crack detection techniques for Timoshenko E-FGM beam. In the first technique, the frequency contours with respect to crack location and size are plotted and the intersection of contours of different modes helps in the prediction of crack location and size. The second technique based on response surface methodology and genetic algorithm. Nazari and Abolbashari [22] proposed a procedure for the identification of double cracks E-FGM cantilever beam using artificial neural network (ANN) based on FEM data. The authors used FEM for evaluation of first four natural frequencies for different cracks depths and locations. The trained ANNs are used for identification of cracks locations and depths of considered beam. The proposed procedure can predict the cracks locations and depths of double cracked FGM beam accurately. Furthermore, the crack locations were predicted more accurately than the crack depths using ANNs. Khiem and Huyen [23] proposed a method to detect a single crack in FGM Timoshenko beam by measurements of three lowest natural frequencies. The frequency equations are conducted on the base of power law of FGM, taking into account the actual position of neutral axis and rotational spring model of crack. Unlikely to the previous studies, where stiffness of only rotational spring representing severity of crack is calculated not for every composition of FGM, in this study, new formulas for determining crack magnitude of both the translational and rotational springs are proposed for arbitrary composition of FGM.

Among the numerous proposed Non-Destructive Testing (NDT) methods [24] the wavelet-based approach shows to be the most effective, especially for detecting the small local damage such as crack in structures. However, the most of the published works have been devoted to apply the wavelet transform for crack detection in beam-like structures made of homogeneous materials. Surace and Ruotolo [25] stated that presence of a crack in a cantilever beam can be detected by the wavelet coefficient distribution computed from the time history response measured at free end. Liew and Wang [26] demonstrated that single crack in a simply supported beam can be localized from spatial wavelet transform of free vibration response measured along the beam length at a given time moment. This study was then continued by Wang and Deng [27] for the case of impulse response of beam and plate with different boundary conditions. Douka et al. [28] have achieved at identifying both the location and size of single crack in a cantilever beam by using the wavelet coefficient distribution along the beam length of the fundamental mode shape. The crack depth is estimated by so-called the intensity factor related to the wavelet maxima coefficient. Chang and Chen [29] have proposed a method for estimating both the position and depth of multiple cracks in beam based on the spatial wavelet transform of mode shapes. The crack depth evaluation has been simplified by using the estimated crack positions and available natural frequencies. This idea was then extended by Zhang

et al. [30] to multiple crack detection for stepped beam with involved the transfer matrix method. Zhong and Oyadiji [31] demonstrated that the stationary wavelet transform (SWT) is a useful tool for crack detection from only the mode shape of cracked beam-like structure. Gokdag and Kopmaz [32] have proved that the approximation component of the wavelet decomposition is similar to the mode shape of undamaged structure so that it can be employed as the base-line data for conducting a damage index based on differences of the wavelet coefficients. Lien, Khiem and Hao [33] proposed a method based on the SWT for crack identification in framed structures. First, the DSM was developed to conduct the more accurate dynamic model of multiple cracked frame structures that allows for obtaining mode shapes. Then, the SWT was applied for crack detection from spatial wavelet coefficient of the structure mode shapes. The illustrating numerical results verify that the developed dynamic model of cracked frame structures combined with the SWT can be reliably employed for localization of cracks in frame structures with data contaminated with noise of SNR from 75 dB.

To the best of the authors' knowledge, the wavelet based approach to the crack identification of multiple cracked FGM beam is a gap that has to be fulfilled. In this paper, crack identification of multiple cracked FGM beam by using SWT of mode shapes is addressed. First, the DSM is presented to conduct the more accurate dynamic model of multiple cracked P-FGM beam that allows for obtaining mode shapes. Then, the SWT is applied for crack identification from spatial wavelet coefficient of the structure mode shapes. The theoretical development was illustrated and validated by numerical examples. A case study has been accomplished to investigate also the influence of measurement noise on the wavelet coefficients.

2. DETERMINATION OF MODE SHAPES OF A MULTIPLE CRACKED FGM BEAM ELEMENT BY USING DSM

2.1. Governing equations

Consider a FGM beam of length L, cross sectional area $A = b \times h$ (Fig. 1). It is assumed that the material properties of FGM beam vary along the thickness direction by the power law distribution (P-FGM) as follows

$$\left\{ \begin{array}{c} E(z) \\ G(z) \\ \rho(z) \end{array} \right\} = \left\{ \begin{array}{c} E_b \\ G_b \\ \rho_b \end{array} \right\} + \left\{ \begin{array}{c} E_t - E_b \\ G_t - G_b \\ \rho_t - \rho_b \end{array} \right\} \left(\frac{z}{h} + \frac{1}{2} \right)^n \ ; \ -h/2 \leq z \leq h/2, \qquad (1)$$
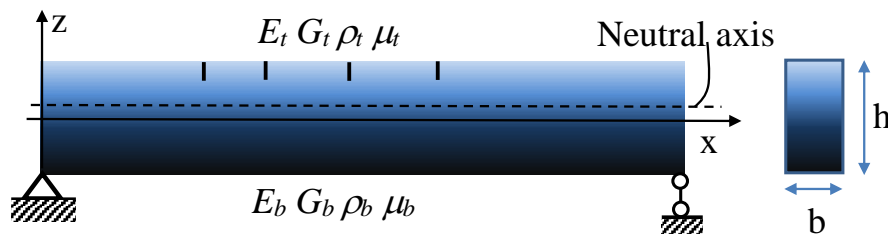

Fig. 1. A multiple cracked FGM beam

where E, G and ρ stand for Young's, shear modulus and material density; subscripts t and b denote the top and bottom material; n is power law exponent; z is coordinate of point from the mid plane of the beam. Assuming small deformation, the displacement at a point in the section of Timoshenko beam is

$$u(x,z,t) = u_0(x,t) - (z - h_0)\theta(x,t), \quad w(x,z,t) = w_0(x,t), \tag{2}$$

where $u_0(x,t), w_0(x,t)$ are axial displacement, deflection of a point on neutral axis, respectively; h_0 is the distance from neutral axis to x-axis; θ is the rotation of the cross-section. Based on the Hamilton's principle, the free vibration equations of FGM Timoshenko beam can be established in the time domain as follow [18]

$$\begin{aligned} (I_{11}\ddot{u}_0 - A_{11}u_0'') - (I_{12}\ddot{\theta} - A_{12}\theta'') &= 0, \\ (I_{12}\ddot{u}_0 - A_{12}u_0'') - (I_{22}\ddot{\theta} - A_{22}\theta'') + A_{33}(w_0' - \theta) &= 0, \\ I_{11}\ddot{w}_0 - A_{33}(w_0'' - \theta') &= 0, \end{aligned} \tag{3a}$$

where

$$(A_{11}, A_{12}, A_{22}) = \int_A E(z)\left(1, z - h_0, (z - h_0)^2\right) dA, \quad A_{33} = \eta \int_A G(z)dA,$$

$$(I_{11}, I_{12}, I_{22}) = \int_A \rho(z)\left(1, z - h_0, (z - h_0)^2\right) dA. \tag{3b}$$

The following notations are introduced

$$\{\mathbf{z}\} = \{U, \Theta, W\}^T = \int_{-\infty}^{\infty} \{u_0(x,t), \theta(x,t), w_0(x,t)\}^T e^{-i\omega t}dt, \tag{4}$$

where $\{U, \Theta, W\}$ are respectively the amplitudes of axial displacement, rotation and deflection. We get the free vibration equations of FGM Timoshenko beam in the frequency domain as follow

$$[\tilde{\mathbf{A}}]\{\mathbf{z}''\} + [\tilde{\mathbf{\Pi}}]\{\mathbf{z}'\} + [\tilde{\mathbf{D}}]\{\mathbf{z}\} = \{0\}, \tag{5a}$$

where

$$[\tilde{\mathbf{A}}] = \begin{bmatrix} A_{11} & -A_{12} & 0 \\ -A_{12} & A_{22} & 0 \\ 0 & 0 & A_{33} \end{bmatrix}, \quad [\tilde{\mathbf{\Pi}}] = \begin{bmatrix} 0 & 0 & 0 \\ 0 & 0 & A_{33} \\ 0 & -A_{33} & 0 \end{bmatrix},$$

$$[\tilde{\mathbf{D}}] = \begin{bmatrix} \omega^2 I_{11} & -\omega^2 I_{12} & 0 \\ -\omega^2 I_{12} & \omega^2 I_{22} - A_{33} & 0 \\ 0 & 0 & \omega^2 I_{11} \end{bmatrix}. \tag{5b}$$

The solutions of equation (5) can be now rewritten in the form

$$\{\mathbf{z}_0(x,\omega)\} = [\mathbf{G}(x,\omega)]\{\mathbf{C}\}, \tag{6}$$

where $[\mathbf{G}(x,\omega)]$ is matrix of dimension 3×6

$$[\mathbf{G}(x,\omega)] = \begin{bmatrix} \alpha_1 e^{k_1 x} & \alpha_2 e^{k_2 x} & \alpha_3 e^{k_3 x} & \alpha_1 e^{-k_1 x} & \alpha_2 e^{-k_2 x} & \alpha_3 e^{-k_3 x} \\ e^{k_1 x} & e^{k_2 x} & e^{k_3 x} & e^{-k_1 x} & e^{-k_2 x} & e^{-k_3 x} \\ \beta_1 e^{k_1 x} & \beta_2 e^{k_2 x} & \beta_3 e^{k_3 x} & -\beta_1 e^{-k_1 x} & -\beta_2 e^{-k_2 x} & -\beta_3 e^{-k_3 x} \end{bmatrix}, \tag{7}$$

$k_i, \lambda_i, \beta_i (i = 1, 2, 3)$ are constants determined in Appendix 1 and $\{\mathbf{C}\} = (C_1, \ldots, C_6)^T$ is unknown constant vector determined from boundary conditions.

It is assumed that the beam has been cracked at position e. The crack is modeled as two springs: an axial spring of stiffness T and a rotational spring of stiffness R (Fig. 2). The continuous conditions of the crack are [3,15]

$$U(e+0) = U(e-0) + \gamma_1 U'(e), \ \Theta(e+0) = \Theta(e-0) + \gamma_2 \Theta'(e), \ W(e+0) = W(e-0),$$
$$U'(e+0) = U'(e-0), \ \Theta'(e+0) = \Theta'(e-0), \ W'(e+0) = W'(e-0) + \gamma_2 \Theta'(e). \tag{8}$$
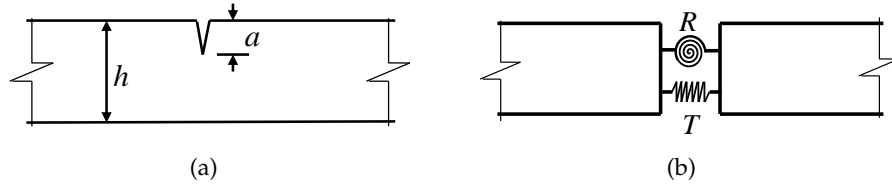
Fig. 2. FGM beam with open edge crack and the model of two equivalent springs

The magnitudes γ_1, γ_2 introduced in (8) are functions of material parameters such as Young's modulus, power exponent, beam height, Poisson coefficient, ... included case of homogeneous beam $E_t = E_b = E_0$ or $R_E = 1$

$$\gamma_1 = A_{11}/T = 2\pi(1 - v^2)h\sigma_1 f_1(s) \ , \ \gamma_2 = A_{22}/R = 6\pi(1 - v^2)h\sigma_2 f_2(s) \ , \ s = a/h, \tag{9}$$

where [23]

$$\sigma_1(R_E, n) = \frac{2(R_E + n)}{(R_E + 1)(1 + n)},$$
$$\sigma_2(R_E, n) = \frac{24}{R_E + 1} \left(\frac{3R_E + n}{3(3 + n)} - \frac{2R_E + n}{2 + n}\alpha + \frac{R_E + n}{1 + n}\alpha^2 \right), \quad R_E = \frac{E_t}{E_b},$$
$$f_1(s) = s^2(0.6272 - 0.17248s + 5.92134s^2 - 10.7054s^3 + 31.5685s^4 - 67.47s^5 \tag{10}$$
$$+ 139.123s^6 - 146.682s^7 + 92.3552s^8),$$
$$f_2(s) = s^2(0.6272 - 1.04533s + 4.5948s^2 - 9.9736s^3 + 20.2948s^4 - 33.0351s^5$$
$$+ 47.1063s^6 - 40.7556s^7 + 19.6s^8).$$

The homogeneous solution $\{\mathbf{z}_e(x)\}$ of (5) that satisfied left boundary conditions

$$\{\mathbf{z}_e(0)\} = (\gamma_1 U'_x(e), \gamma_2 \Theta'_x(e), 0)^T, \quad \{\mathbf{z'}_e(0)\} = (0, 0, \gamma_2 \Theta'_x(e))^T, \tag{11}$$

and

$$\{\mathbf{z'}_0(e)\} = (U'_0(e) \ \Theta'_0(e) \ W'_0(e))^T. \tag{12}$$

We obtain

$$\{\mathbf{z}_e(x)\} = [\mathbf{\Phi}(x)][\mathbf{\Sigma}]\{\mathbf{z'}_0(e)\} = [\mathbf{G}_c(x)]\{\mathbf{z'}_0(e)\}, \tag{13}$$

where $[\mathbf{G}_c(x)]$ is matrix of dimension 3×3

$$[\mathbf{G}_c(x)] = \begin{bmatrix} \alpha_1 \cosh k_1 x & \alpha_2 \cosh k_{21} x & \alpha_3 \cosh k_3 x \\ \cosh k_1 x & \cosh k_{21} x & \cosh k_3 x \\ \beta_1 \sinh k_1 x & \beta_2 \sinh k_2 x & \beta_3 \sinh k_3 x \end{bmatrix} \cdot \begin{bmatrix} \delta_{11} & \delta_{12} & \delta_{13} \\ \delta_{21} & \delta_{22} & \delta_{23} \\ \delta_{31} & \delta_{32} & \delta_{33} \end{bmatrix} \cdot \begin{bmatrix} \gamma_1 & 0 & 0 \\ 0 & \gamma_2 & 0 \\ 0 & \gamma_2 & 0 \end{bmatrix},$$

$$\begin{aligned} \delta_{11} &= (k_3\beta_3 - k_2\beta_2)/\Delta, & \delta_{12} &= (\alpha_3 k_2\beta_2 - \alpha_2 k_3\beta_3)/\Delta, & \delta_{13} &= (\alpha_2 - \alpha_3)/\Delta, \\ \delta_{21} &= (k_1\beta_1 - k_3\beta_3)/\Delta, & \delta_{22} &= (\alpha_1 k_3\beta_3 - \alpha_3 k_1\beta_1)/\Delta, & \delta_{23} &= (\alpha_3 - \alpha_1)/\Delta, \\ \delta_{31} &= (k_2\beta_2 - k_1\beta_1)/\Delta, & \delta_{32} &= (\alpha_2 k_1\beta_1 - \alpha_1 k_2\beta_2)/\Delta, & \delta_{33} &= (\alpha_1 - \alpha_2)/\Delta, \end{aligned} \quad (14)$$

$$\Delta = k_1\beta_1(\alpha_2 - \alpha_3) + k_2\beta_2(\alpha_3 - \alpha_1) + k_3\beta_3(\alpha_1 - \alpha_2).$$

We introduce matrix of crack functions

$$[\bar{G}(x)] = \begin{cases} [\mathbf{G}_c(x)] & : \quad x > 0 \\ [\mathbf{0}] & : \quad x \leq 0 \end{cases} \quad (15)$$

For multiple cracked beam, we can present solutions of Eq. (5) in the form [18,19]

$$\{\mathbf{z}_c(x)\} = \{\mathbf{z}_0(x)\} + \sum_{j=1}^{n} [\bar{\mathbf{G}}(x - e_j)] \cdot \{\boldsymbol{\mu}_j\}, \quad (16)$$

where $\{\boldsymbol{\mu}_j\}$ is vector of dimension 3×1

$$\{\boldsymbol{\mu}_j\} = \{\mathbf{z}'_0(e_j)\} + \sum_{k=1}^{j-1} [\bar{\mathbf{G}}'(e_j - e_k)] \cdot \{\boldsymbol{\mu}_k\}, \quad j = 1, 2, 3, \ldots, n \quad (17)$$

Suppose that boundary conditions for solution of Eq. (5), are represented by

$$\{\mathbf{B}_0(\mathbf{z}_c)|_{x=0}\} = \{\mathbf{0}\}, \quad \{\mathbf{B}_L(\mathbf{z}_c)|_{x=L}\} = \{\mathbf{0}\}, \quad (18)$$

where $[\mathbf{B}_0]$, $[\mathbf{B}_L]$ differential matrix operators of dimension 3×3 (see Appendix 2). Since the second term of solution (16) satisfies any trivial condition at $x = 0$, the first condition in (18) is only applied for $\mathbf{z}_0(x)$. Splitting the vector $\mathbf{C} = \{\mathbf{C}_0, \mathbf{C}_L\}^T$ into $\mathbf{C}_0 = \{C_1, C_2, C_3\}^T; \mathbf{C}_L = \{C_4, C_5, C_6\}^T$, the boundary condition at the left of the beam can be rewritten as

$$[\mathbf{B}_{01}] \{\mathbf{C}_0\} + [\mathbf{B}_{02}] \{\mathbf{C}_L\} = \{\mathbf{0}\}, \quad (19)$$

with

$$[\mathbf{B}_{01}(\omega)] = [\mathbf{B}_0(\mathbf{G}_1(x, \omega))|_{x=0}], \quad [\mathbf{B}_{02}(\omega)] = [\mathbf{B}_0(\mathbf{G}_2(x, \omega))|_{x=0}]. \quad (20)$$

Eq. (19) allows eliminating one of the vectors $\{\mathbf{C}_0\}$, $\{\mathbf{C}_L\}$ and as the result, the solution $\{\mathbf{z}_0(x)\}$ can be reassembled as

$$\{\mathbf{z}_0(x, \omega)\} = \left(-[\mathbf{G}_1(x, \omega)] \cdot [\mathbf{B}_{01}]^{-1} \cdot [\mathbf{B}_{02}] + [\mathbf{G}_2(x, \omega)] \right) \cdot \{\mathbf{C}_L\} = [\mathbf{G}_0(x, \omega)] \{\mathbf{C}_L\}. \quad (21)$$

Substituting (21) into (16) we obtain

$$\{\mathbf{z}_c(x)\} = \left([\mathbf{G}_0(x)] + \sum_{j=1}^{n} [\bar{\mathbf{G}}(x - e_j)] \cdot [\boldsymbol{\chi}_j] \right) \cdot \{\mathbf{C}_L\} = [\mathbf{G}_L(x, \omega)] \cdot \{\mathbf{C}_L\}, \quad (22)$$

where

$$[\mathbf{G}_L(x,\omega)] = [\mathbf{G}_0(x)] + \sum_{j=1}^{n} [\bar{\mathbf{G}}(x-e_j)] \cdot [\chi_j], \tag{23}$$

and

$$[\chi_j] = [\mathbf{G}'_0(e_j)] + \sum_{k=1}^{j-1} [\bar{\mathbf{G}}'(e_j - e_k)] \cdot [\chi_k], \quad j = 1,2,3,\ldots,n \tag{24}$$

Satisfying boundary condition at right end of the beam leads to

$$[\mathbf{B}_{LL}\omega)]\{\mathbf{C}_L\} = \{\mathbf{0}\},$$

where

$$[\mathbf{B}_{LL}(\omega)] = [\mathbf{B}_L(\mathbf{G}_L(x,\omega))\,|_{x=L}]. \tag{25}$$

We obtain the frequency equation for FGM beam with arbitrary number of cracks

$$\Lambda(\omega) = \det[\mathbf{B}_{LL}(\omega)] = 0. \tag{26}$$

The mode shape relating to natural frequency ω_j is

$$\{\phi_j(x)\} = \bar{c}_j [\mathbf{G}_L(x,\omega_j)] \{\bar{\mathbf{C}}_j\}, \tag{27}$$

where $\bar{c}_j$ is an arbitrary constant and $\{\bar{\mathbf{C}}_j\}$ is the normalized solution of (26) corresponding to ω_j.

2.2. Wavelet transform and stationary wavelet transform

Wavelet transform starts by selecting a basis function from wavelet families. This function is called "mother wavelet" $\psi(x)$. The continuous wavelet transform (CWT) is then defined as [34–36]

$$C(a,b) = \frac{1}{\sqrt{a}} \int_{-\infty}^{\infty} f(x)\,\psi\left(\frac{x-b}{a}\right) dx = \int_{-\infty}^{\infty} f(x)\,\psi_{a,b}(x)\,dx, \tag{28}$$

where $a > 0$ and b are dilation scale and transition parameter; $\psi_{a,b}(x)$ is function

$$\psi_{a,b}(x) = \frac{1}{\sqrt{a}}\psi\left(\frac{x-b}{a}\right). \tag{29}$$

The result of CWT is wavelet coefficients $C(a,b)$ showing the correlations between the wavelet function and the signal analyzed $f(x)$. Hence, sharp transitions in $f(x)$ create wavelet coefficients with large amplitude and this precisely is the basis of the proposed identification method.

The initial signal $f(x)$ can be reconstructed from the wavelet coefficients $C(a,b)$

$$f(x) = \frac{1}{K_{\psi}} \int_{-\infty}^{\infty} \int_{-\infty}^{\infty} C(a,b)\,\psi_{a,b}(x)\frac{db\,da}{a^2}, \tag{30}$$

where the constant K_{ψ} depends on wavelet type.

Assuming that wavelet coefficients $C(a,b)$ are valid only for $a < a_0$, appropriate for high-frequency components in the signal, for $a > a_0$, seen as interference. In this case, the

signal reconstruction needs the complement corresponding to $a > a_0$. To do this, another function $\phi(x)$ called "scaling function" is used

$$D(a_0, b) = \frac{1}{\sqrt{a_0}} \int\limits_{-\infty}^{\infty} f(x) \phi\left(\frac{x-b}{a_0}\right) \mathrm{d}x = \int\limits_{-\infty}^{\infty} f(x) \phi_{a_0,b}(x) \mathrm{d}x. \tag{31}$$

The scaling function is necessary for numerical implementation. Instead of (30), the initial signal $f(x)$ can be reconstructed from

$$f(x) = \frac{1}{K_\psi} \int\limits_{a=0}^{a_0} \int\limits_{b=-\infty}^{\infty} C(a,b)\, \psi_{a,b}(x) \frac{\mathrm{d}b\mathrm{d}a}{a^2} + \frac{1}{K_\psi a_0} \int\limits_{b=-\infty}^{\infty} D(a_0, b)\, \phi_{a_0,b}(x)\mathrm{d}b. \tag{32}$$

One drawback of the CWT is that a very large number of wavelet coefficients $C(a,b)$ are generated during the analysis. In order to reduce the amount of computation, the discrete wavelet transform (DWT) used discrete scale and translation parameters in dyadic form: $a = 2^j, b = k2^j$ where j and k are integers, the integer j is referred to as the dyadic level. And the DWT is as follows

$$C_{j,k} = 2^{-j/2} \int\limits_{-\infty}^{\infty} f(x) \psi\left(2^{-j}x - k\right) \mathrm{d}x = \int\limits_{-\infty}^{\infty} f(x) \psi_{j,k}(x) \mathrm{d}x, \tag{33}$$

where $\psi_{j,k}(x)$ is discrete wavelet function

$$\psi_{j,k}(x) = 2^{-j/2}\psi\left(2^{-j}x - k\right). \tag{34}$$

Instead of (30), the signal in DWT can be reconstructed from the wavelet coefficients $C_{j,k}$

$$f(x) = \sum_{j=-\infty}^{\infty} \sum_{k=-\infty}^{\infty} C_{j,k} 2^{-j/2}\psi\left(2^{-j}x - k\right). \tag{35}$$

The signal will be passed through a series of filters, the high-pass filters and low-pass filters, to generate high-frequency and low-frequency components, respectively. Instead of (32), the signal in DWT can be represented by approximations and details

$$f(x) = \sum_{j=-\infty}^{J} \left(\sum_{k=-\infty}^{\infty} cD_j(k)\, \psi_{j,k}(x)\right) + \sum_{k=-\infty}^{\infty} cA_J(k)\, \phi_{j,k}(x) = \sum_{j \leq J}^{D_j(x)} + A_j(x), \tag{36}$$

where $A_j(x)$ is the approximation at level J; $D_j(x)$ is the detail at level $j \leq J$

$$D_j(x) = \sum_{k=-\infty}^{\infty} cD_j(k)\, \psi_{j,k}(x), \quad A_j(x) = \sum_{k=-\infty}^{\infty} cA_J(k)\, \phi_{j,k}(x), \tag{37}$$

cD_j and cA_j are detail coefficient and approximation coefficient, respectively

$$cD_J(k) = \int\limits_{-\infty}^{\infty} f(x) \psi_{J,k}(x) \mathrm{d}x, \quad cA_J(k) = \int\limits_{-\infty}^{\infty} f(x) \phi_{J,k}(x) \mathrm{d}x. \tag{38}$$

For this study, we are interested in the detail signal. It will be shown with the numerical examples, if $f(x)$ is response signal, typically the deflection curve, the signal $D_j(x)$ contain the information necessary to detect the cracks in the structure.

But the classical DWT suffers a drawback that is not a time-invariant transform. This means that, even with periodic signal extension, the DWT of a translated version of the original signal is not, in general, the translated version of the DWT of the original signal. To circumvent this problem, one can resort to a redundant decomposition of signal as [31]

$$\tilde{D}_{j,k} = 2^{-j/2} \int\limits_{-\infty}^{\infty} f(x)\, \psi\left(\frac{x-k}{2^j}\right) \mathrm{d}x, \quad \tilde{A}_{j,k} = 2^{-j/2} \int\limits_{-\infty}^{\infty} f(x)\, \phi\left(\frac{x-k}{2^j}\right) \mathrm{d}x. \quad (39)$$

The modified approximation and detail coefficients (39) constitute the so-called SWT that has a great potential in signal processing for structural health monitoring. It should be noted that the SWT of the origin data is not decimated. That is, the size of the SWT data does not diminish after the transform. In fact, SWT doubles the number of input samples at each iteration, which can provide a more accurate estimate of the variances at each scale and facilitate the identification of salient features in a signal, especially for recognising noise or signal rupture. Conversely, in DWT, the resulting transformed data is half of the original signal size. Thus, DWT is a down-sampling process which results in a poorer representation of the original signal. Conversely, SWT is an up-sampling process which leads to redundant representation of the original signal. Therefore, the detail coefficient of DWT decomposition has less feature information than that of SWT. Consequently, SWT has great potential for feature extraction and facilitates the identification of salient features in a signal.

2.3. Noise and reduction of noise

In real case, the true mode shape data of a cracked structure can be expressed approximately as [31]

$$y = y_{\text{int } act} + y_{noise} + y_{crack}, \quad (40)$$

where y is the measured mode shape data; $y_{\text{int } act}$ is the mode shape of uncracked structure without any noise contamination; y_{noise} is the response noise which is either numerical noise (in the case of numerical computations of mode shape data) or experimental noise (in the case of experimental measurement of mode shape data) and exists both in uncracked and cracked beams; y_{crack} is the additional response due to the crack and exists only in the cracked beams.

Theoretically, the true mode shape data can be decomposed by SWT into two parts: one called approximation coefficient contains $y_{\text{int } act}$, which is a smooth curve; the other called detail coefficient consists of y_{noise} and y_{crack}. It is noted here that the response noise of uncracked beam or cracked beam are both included in the detail coefficient. In order to reduce the response due to the crack accurately and, thereby facilitate crack detection, proper methods should be selected to reduce the response noise of uncracked beam or cracked beam.

Usually, the SWT de-noising is achieved via thresholding. There are two threshold-ing methods frequently used: hard-thresholding and soft-thresholding functions. But the soft-thresholding rule is normally chosen over hard-thresholding in de-noising [37].

The hard-thresholding function is defined as

$$\eta_{th} = \begin{cases} x, & |x| > th \\ 0, & |x| < th \end{cases} \quad \text{where } th \text{ is the threshold} \tag{41}$$

The general soft-thresholding function is defined as

$$\eta_{th} = \text{sgn}(x) \max(|x| - th, 0). \tag{42}$$

The following threshold function *th* was used in this paper

$$th = \sigma \sqrt{2 \log N}, \tag{43}$$

where N is the signal length and σ is the standard deviation of the noise.

In case of cracked and uncracked structures, there is noise in both low and high frequencies. For the cracked structures, noise doesn't effect to the signal in additional detail coefficients due to the cracks. So in structure crack identification, effects of noise level on low frequencies will be ignored and we consider it in approximate coefficients of wavelet transformation, and it doesn't effect crack identification by detail coefficients.

To image the experimentally measured data, we add Gaussian noise to mode shapes of structures [35]

$$f(x) = \frac{1}{\sigma \sqrt{2\pi}} e^{-\frac{(x-\mu)^2}{2\sigma^2}} \tag{44}$$

Gaussian curvature is normally depended on expectancy value μ and variance σ^2, or is evaluated by SNR (Signal to Noise Ratio)

$$\text{SNR} = 20 \log_{10} \left(\frac{norm\,(\text{Signal})}{norm\,(\text{Noise})} \right), \quad (\text{dB}) \tag{45}$$

where *norm* is measured criterion of signal $f(x)$ with the length of N_s

$$norm\,(f) = \left(\sum_{i=1}^{N_s} |f(x_i)|^2 \right)^{1/2}, \tag{46}$$

N_s are shift points of the signal pattern $f(x)$. High SNR values correspond to small noise and vice versa. So the noise signal vector in the form of

$$y_{noise} = \frac{y_{nr}}{norm\,(y_{nr})} \cdot \frac{norm\,(y_{\text{int act}})}{10^{(0.05 \times \text{SNR})}}, \tag{47}$$

where $Y_{nr} = \text{Rand}(\text{size}(y_{\text{int act,std}}))$ is random imaged vectors evenly distributed in $(0, 1)$, with the length of base-line signal.

3. NUMERICAL RESULTS AND DISCUSSION

Consider a simply supported FGM beam with material parameters: $E_t = 70$ GPa; $\rho_t = 2780$ kg/m^3; $\mu_t = 0.33$; $E_b/E_t = 0.5$; $\rho_b = 7850$ kg/m^3; $\mu_b = 0.33$; $n = 0.5$ and geometric parameters: $L = 1.0$ m, $b = 0.1$ m, $h = 0.1$ m.
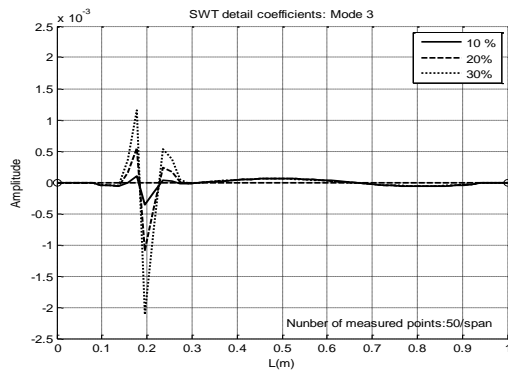
3.1. Effects of cracks

Fig. 3 shows wavelet detail coefficients SWT style *db4* of the first three mode of FGM beam that has 1 crack at location $x_1 = 0.2$ m from the left node, crack depths are 10%, 20% and 30% with number of measured points of 50 points (Figs. 3(a)–3(c)), 100 points (Figs. 3(d)–3(f)), 200 points (Figs. 3(g)–3(i)). From now on, we assume that the number of measured points are 100 points.
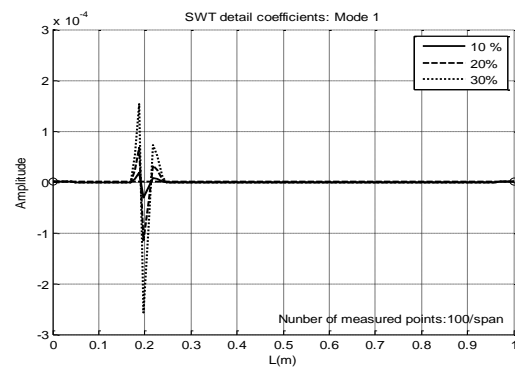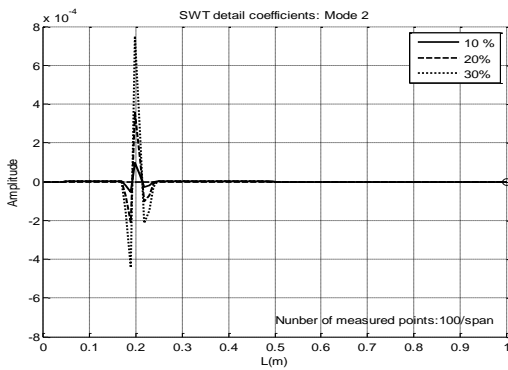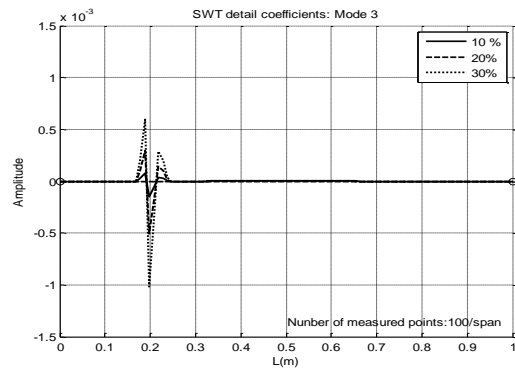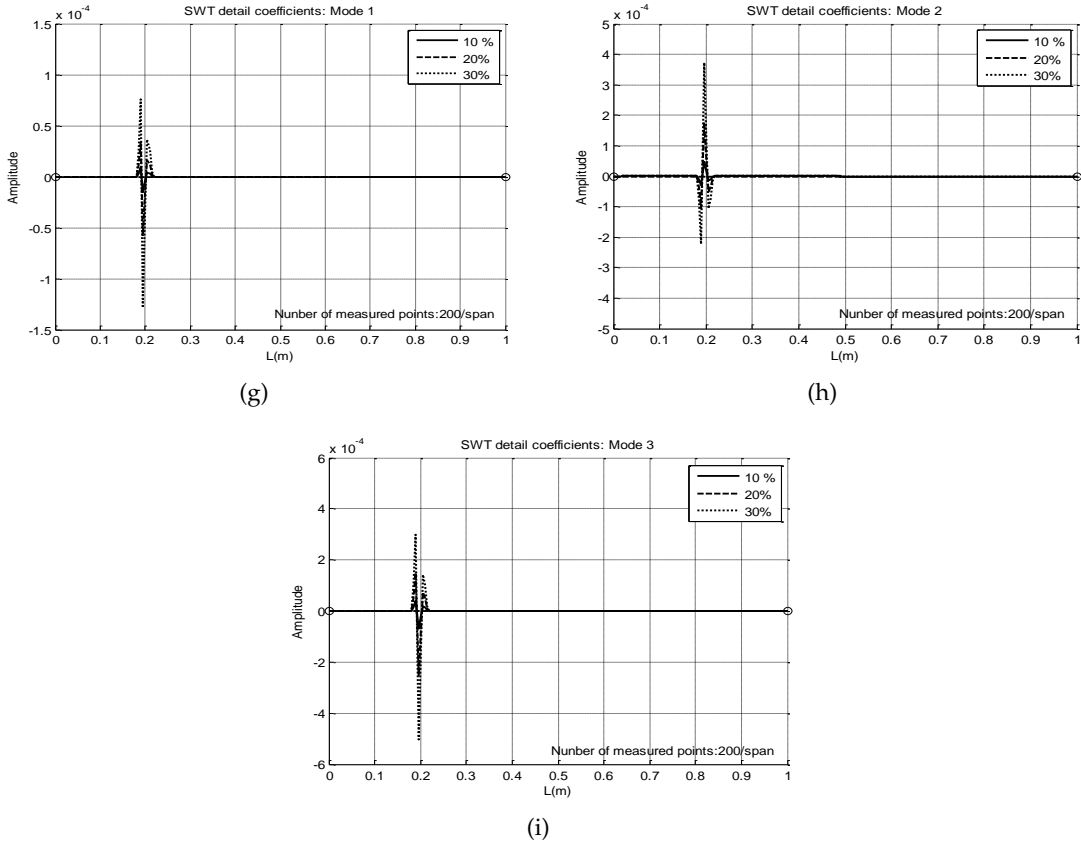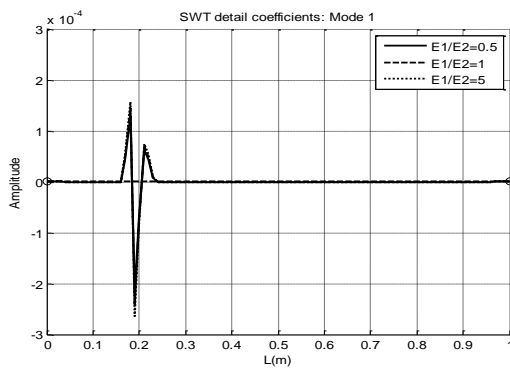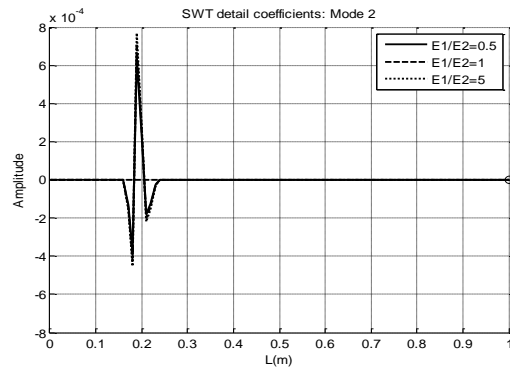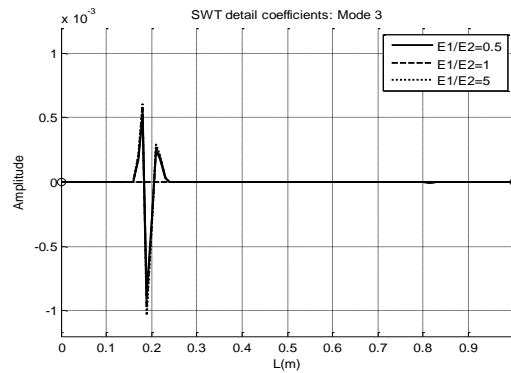

(a)

(b)

(c)

(d)

(e)

(f)

(g)   (h)

(i)
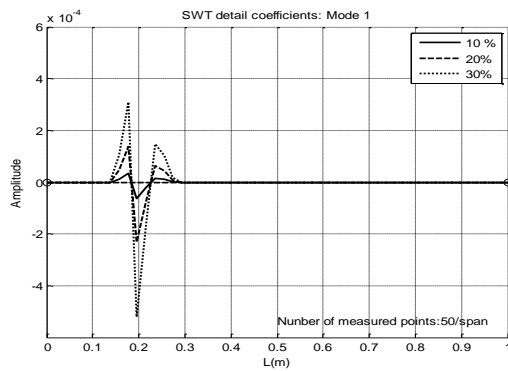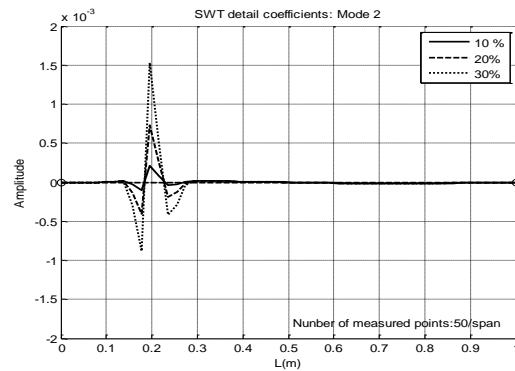
Fig. 3. Wavelet detail coefficients SWT of the first three mode shapes of FGM beam that has
1 crack at 0.2 m, crack depths are 10%, 20%, 30% with number of measured points
of 50(a–c), 100(d–e), 200(g–i)

Fig. 4 shows wavelet detail coefficients SWT style *db4* of the first three mode of FGM
beam that has 1 crack at location $x_1 = 0.2$ m from the left node, crack depth is 30% and

(a)   (b)
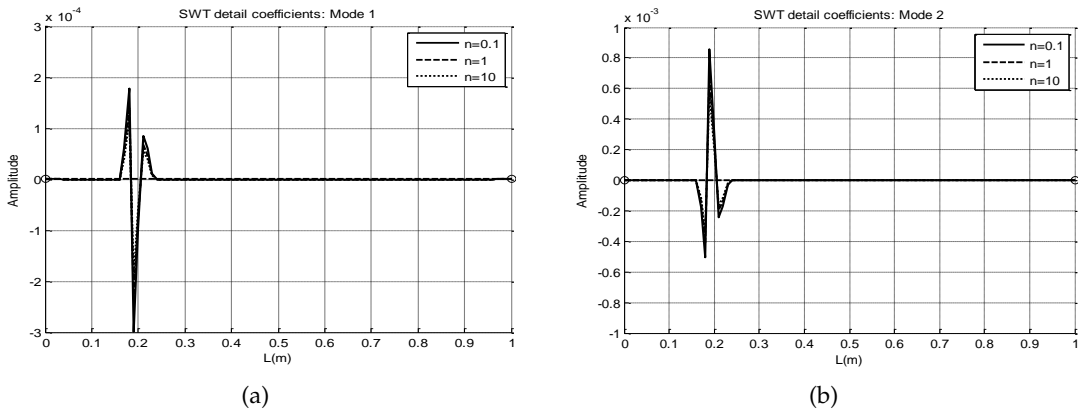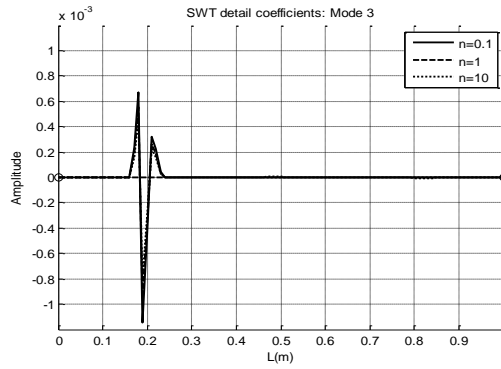
(c)

Fig. 4. Wavelet detail coefficients SWT of the first three mode shapes of FGM beam that
has 1 crack at 0.2 m, crack depth is 30% and power law indexes are $n = 0.1, 1, 10$

(a)

(b)

(c)

Fig. 5. Wavelet detail coefficients SWT of the first three mode shapes of FGM beam that
has 1 crack at 0.2 m, crack depth is 30% and E_t/E_b are 0.5, 1, 5

the power law indexes n are $n = 0.1, 1, 10$. Fig. 5 shows wavelet detail coefficients SWT
style *db4* of the first three mode of FGM beam that has 1 crack at location $x_1 = 0.2$ m

from the left node, crack depth is 30% and E_t/E_b are 0.5, 1, 5. Fig. 6 shows wavelet detail coefficients SWT style *db4* of the first three mode of FGM beam that has 4 equivalent cracks with the distance between cracks are 0.2 m, the crack depths are 10%, 20% and 30%.

(a)

(b)

(c)
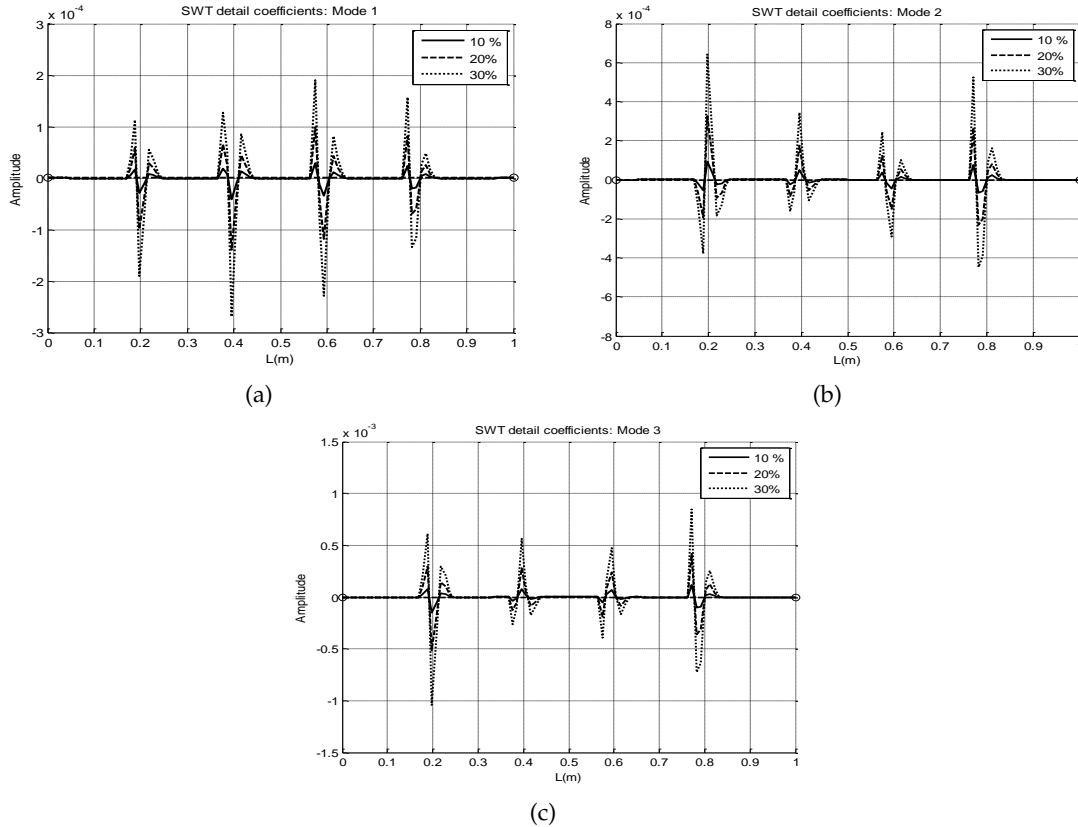
Fig. 6. Wavelet detail coefficients SWT of the first three mode shapes of FGM beam that has 4 equivalent cracks with the crack depth of 10%, 20%, 30%

We have remarks:

- The graphs of wavelet detail coefficients of all the shape modes change suddenly at crack positions. It means that crack position can be more clearly detected using only one mode shape of the cracked beam. It is shown that the crack positions can be identified by showing peaks at the positions of the crack even though the positions of the cracks are very close.

- The present method is very sensitive to the crack depth. The maximum values of wavelet detail coefficients increase when crack depths are bigger. It means that crack position can be more clearly detected with deeper cracks.

- When the beam containing multiple cracks, the same depth cracks located at different positions on beam have different wavelet detail coefficient values. Higher values correspond to crack positions that make the mode shapes changed more. That is because

of the jumps in slope at different crack positions are different even though the crack depths are the same. So the maximum value of wavelet detail coefficients depends not only on the crack depths but also on the crack postions.

- When the number of measured points increases, the effects of crack depths almost are the same, but the absolute value of wavelet detail coefficients increase remarkably and the transformation zones become narrower.

- When power law index n decreases or E_t/E_b ratio increases, the beam is more sensitive to presence of cracks, wavelet detail coefficients are highly increased.

We also have the similar remarks for a cracked beam with different boundary condition such as cantilever beam, clamped ends, ...

3.2. Effects of different noise level

Input signals are the first three mode shapes of cracked FGM beam added by different SNR noise levels. Fig. 7 shows wavelet detail coefficients SWT of the fundamental mode shape (Figs. 7(a)–7(c)), the second mode shape (Figs. 7(d)–7(f)) and the third mode shape (Figs. 7(g)–7(i)) of simply supported FGM beam and SNR noise level at 75, 80 and 90 dB. Fig. 8 shows wavelet detail coefficients SWT style db4 of the first three mode shapes of the simple support FGM beam that has 4 equivalent cracks at 0.2 m, 0.4 m, 0.6 m, 0.8 m from the left node with the depth of 30% and noise level of 75, 80 and 90 dB. It can be seen that the crack position can be clearly detected by using fundamental mode
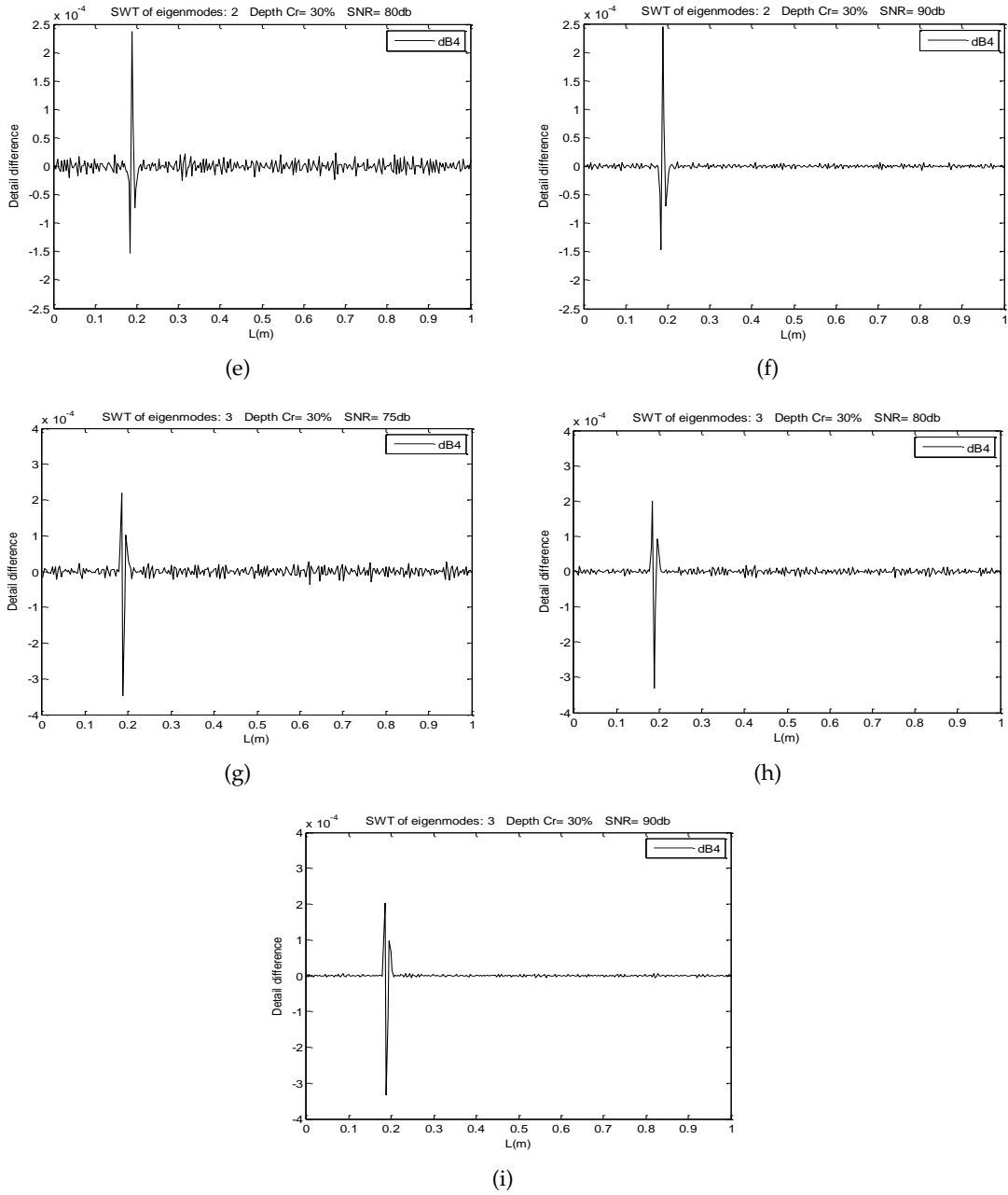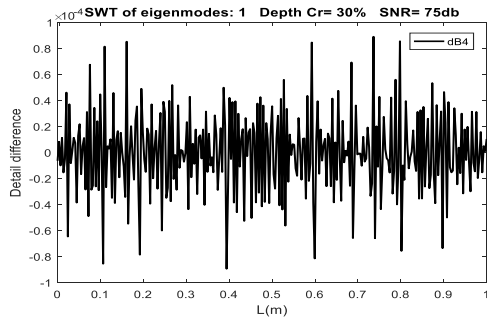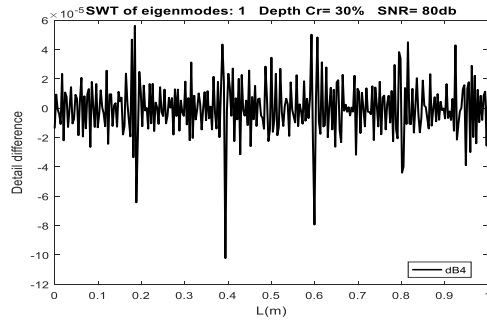

(a)

(b)

(c)

(d)

(e)

(f)

(g)

(h)

(i)
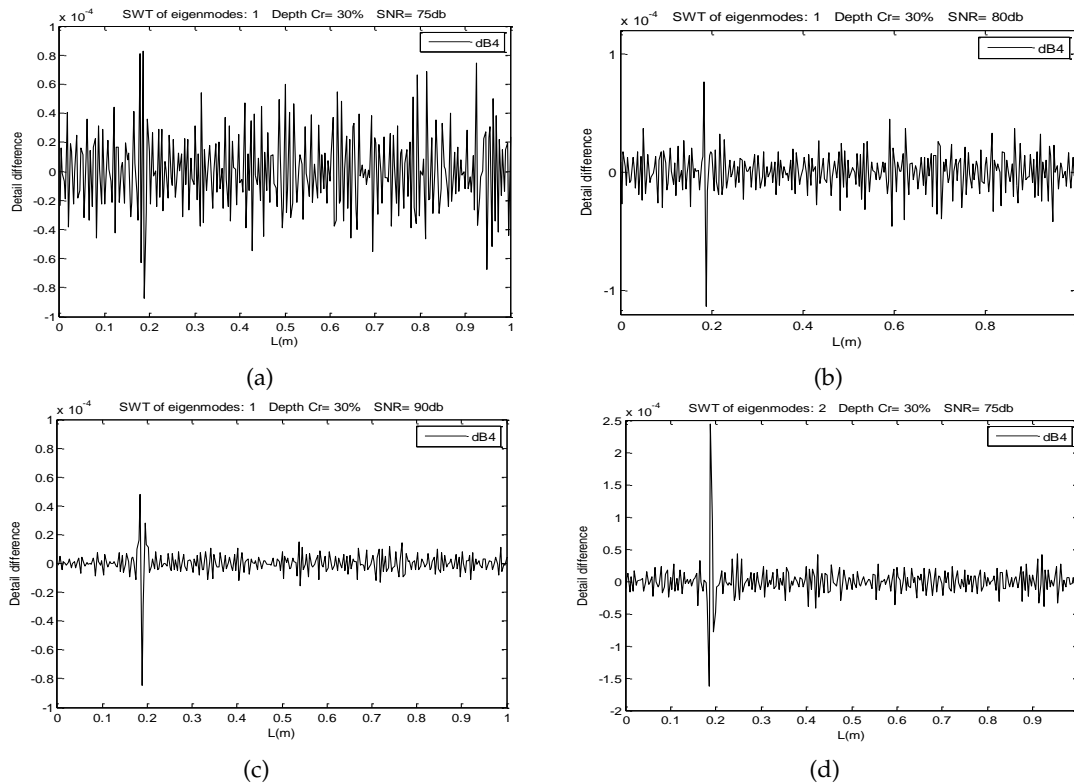
Fig. 7. Wavelet detail coefficients SWT of the first three mode shapes of FGM beam that has 1 crack at 0.2 m from the left node with the depth of 30% and noise level 75, 80 and 90 dB
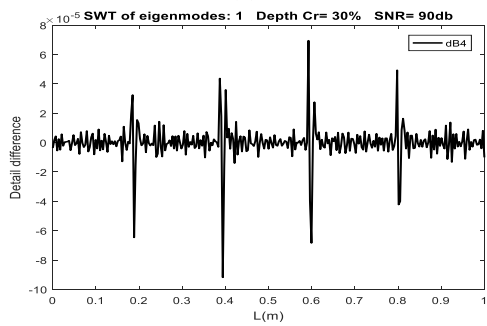
shape if the SNR exceeds 80 dB (Figs. 7(b) and 8(b)), using the second and third mode shapes if the SNR exceeds 75 dB (Figs. 7(d) and 8(d)).
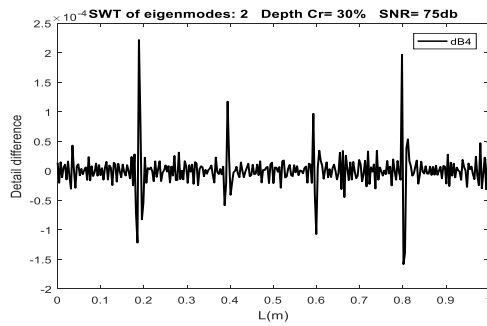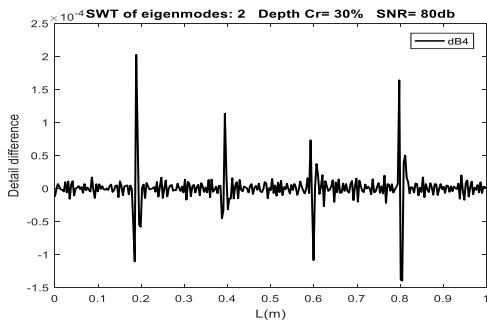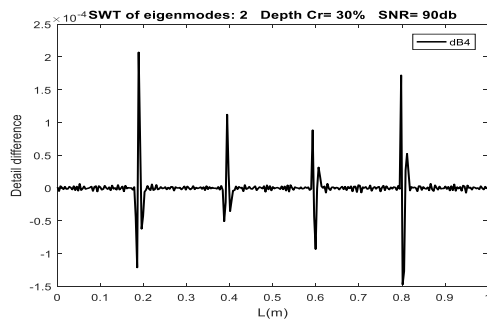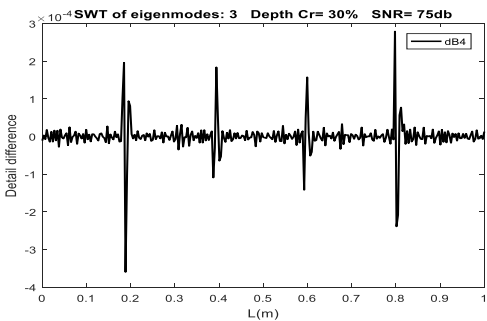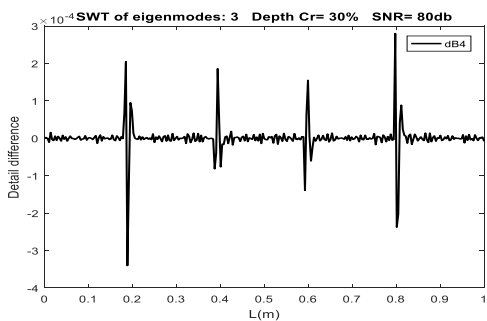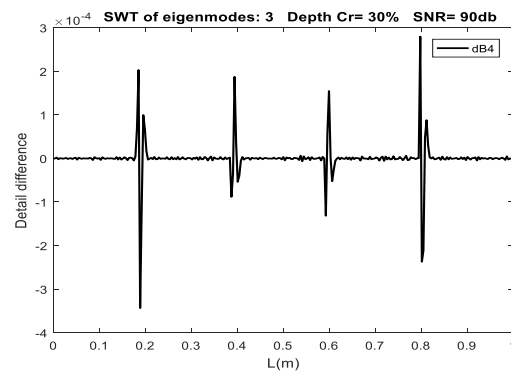
(a)

(b)

(c)

(d)

(e)

(f)

(g)

(h)

(i)

Fig. 8. Wavelet detail coefficients SWT of the first three mode shapes of the simple support FGM beam that has 4 equivalent cracks at 0.2 m, 0.4 m, 0.6 m, 0.8 m from the left node with the depth of 30% and noise level 75, 80 and 90 dB

4. CONCLUSIONS

In this paper, crack identification in a multiple cracked FGM beam by using SWT of mode shapes and taking into account influence of Gaussian noise is addressed. Mode shapes are obtained from the multiple cracked FGM beam element model using DSM and spring model of cracks. Hence, SWT is applied for crack identification of the multiple cracked FGM beam.

Numerical analysis was carried out to validate the proposed method and to investigate effect of cracks, material properties and Gaussian noise on crack identification of a multiple cracked FGM beam. The illustrating numerical results verify that the multiple cracked FGM beam element model combined with the SWT can be reliably employed for localization of cracks in beam-like structures with data contaminated with noise of SNR from 75 dB. Moreover, crack position can be more clearly detected using only one mode shape of the cracked beam. The investigated results show that proposed method is efficient and realizable.

ACKNOWLEDGEMENT

REFERENCES

[1] Z. H. Jin and R. C. Batra. Some basic fracture mechanics concepts in functionally graded materials. *Journal of the Mechanics and Physics of Solids*, **44**, (8), (1996), pp. 1221–1235. https://doi.org/10.1016/0022-5096(96)00041-5.

[2] F. Erdogan and B. H. Wu. The surface crack problem for a plate with functionally graded properties. *Journal of Applied Mechanics*, **64**, (3), (1997), pp. 449–456. https://doi.org/10.1115/1.2788914.

[3] L. L. Ke, J. Yang, S. Kitipornchai, and Y. Xiang. Flexural vibration and elastic buckling of a cracked Timoshenko beam made of functionally graded materials. *Mechanics of Advanced Materials and Structures*, **16**, (6), (2009), pp. 488–502. https://doi.org/10.1080/15376490902781175.

[4] J. Yang, Y. Chen, Y. Xiang, and X. L. Jia. Free and forced vibration of cracked inhomogeneous beams under an axial force and a moving load. *Journal of Sound and Vibration*, **312**, (1-2), (2008), pp. 166–181. https://doi.org/10.1016/j.jsv.2007.10.034.

[5] K. Aydin. Free vibration of functionally graded beams with arbitrary number of surface cracks. *European Journal of Mechanics-A/Solids*, **42**, (2013), pp. 112–124. https://doi.org/10.1016/j.euromechsol.2013.05.002.

[6] J. Yang and Y. Chen. Free vibration and buckling analyses of functionally graded beams with edge cracks. *Composite Structures*, **83**, (1), (2008), pp. 48–60. https://doi.org/10.1016/j.compstruct.2007.03.006.

[7] D. Wei, Y. Liu, and Z. Xiang. An analytical method for free vibration analysis of functionally graded beams with edge cracks. *Journal of Sound and Vibration*, **331**, (7), (2012), pp. 1686–1700. https://doi.org/10.1016/j.jsv.2011.11.020.

[8] K. Sherafatnia, G. Farrahi, and S. A. Faghidian. Analytic approach to free vibration and buckling analysis of functionally graded beams with edge cracks using four engineering beam theories. *International Journal of Engineering-Transactions C: Aspects*, **27**, (6), (2013), pp. 979–990. https://doi.org/10.5829/idosi.ije.2014.27.06c.17.

[9] N. T. Khiem and D. T. Hung. A closed-form solution for free vibration of multiple cracked Timoshenko beam and application. *Vietnam Journal of Mechanics*, **39**, (4), (2017), pp. 315–328. https://doi.org/10.15625/0866-7136/9641.

[10] N. T. Khiem, L. K. Toan, and N. T. L. Khue. Change in mode shape nodes of multiple cracked bar: I. The theoretical study. *Vietnam Journal of Mechanics*, **35**, (3), (2013), pp. 175–188. https://doi.org/10.15625/0866-7136/35/3/2486.

[11] N. T. Khiem, L. K. Toan, and N. T. L. Khue. Change in mode shape nodes of multiple cracked bar: II. The numerical analysis. *Vietnam Journal of Mechanics*, **35**, (4), (2013), pp. 299–311. https://doi.org/10.15625/0866-7136/35/4/2487.

[12] S. Kitipornchai, L. L. Ke, J. Yang, and Y. Xiang. Nonlinear vibration of edge cracked functionally graded Timoshenko beams. *Journal of Sound and Vibration*, **324**, (3-5), (2009), pp. 962–982. https://doi.org/10.1016/j.jsv.2009.02.023.

[13] Z. Yu and F. Chu. Identification of crack in functionally graded material beams using the p-version of finite element method. *Journal of Sound and Vibration*, **325**, (1-2), (2009), pp. 69–84. https://doi.org/10.1016/j.jsv.2009.03.010.

[14] Ş. D. Akbaş. Free vibration characteristics of edge cracked functionally graded beams by using finite element method. *International Journal of Engineering Trends and Technology*, **4**, (10), (2013), pp. 4590–4597.

[15] A. Banerjee, B. Panigrahi, and G. Pohit. Crack modelling and detection in Timoshenko FGM beam under transverse vibration using frequency contour and response surface model with GA. *Nondestructive Testing and Evaluation*, **31**, (2), (2016), pp. 142–164. https://doi.org/10.1080/10589759.2015.1071812.

[16] K. V. Nguyen. Crack detection of a beam-like bridge using 3D mode shapes. *Vietnam Journal of Mechanics*, **36**, (1), (2014), pp. 13–25. https://doi.org/10.15625/0866-7136/36/1/2965.

[17] H. Su and J. R. Banerjee. Development of dynamic stiffness method for free vibration of functionally graded Timoshenko beams. *Computers & Structures*, **147**, (2015), pp. 107–116. https://doi.org/10.1016/j.compstruc.2014.10.001.

[18] T. V. Lien, N. T. Duc, and N. T. Khiem. Free vibration analysis of multiple cracked functionally graded Timoshenko beams. *Latin American Journal of Solids and Structures*, **14**, (9), (2017), pp. 1752–1766. https://doi.org/10.1590/1679-78253693.

[19] T. V. Lien, N. T. Duc, and N. T. Khiem. Mode shape analysis of multiple cracked functionally graded Timoshenko beams. *Latin American Journal of Solids and Structures*, **14**, (7), (2017), pp. 1327–1344. https://doi.org/10.1590/1679-78253496.

[20] N. T. Khiem and T. V. Lien. The dynamic stiffness matrix method in forced vibration analysis of multiple-cracked beam. *Journal of Sound and Vibration*, **254**, (3), (2002), pp. 541–555. https://doi.org/10.1006/jsvi.2001.4109.

[21] T. V. Lien, N. T. Duc, and N. T. Khiem. Mode shape analysis of multiple cracked functionally graded beam-like structures by using dynamic stiffness method. *Vietnam Journal of Mechanics*, **39**, (3), (2017), pp. 215–228. https://doi.org/10.15625/0866-7136/8631.

[22] F. Nazari and M. H. Abolbashari. Double cracks identification in functionally graded beams using artificial neural network. *Journal of Solid Mechanics*, **5**, (1), (2013), pp. 14–21.

[23] N. T. Khiem and N. N. Huyen. A method for crack identification in functionally graded Timoshenko beam. *Nondestructive Testing and Evaluation*, **32**, (3), (2017), pp. 319–341. https://doi.org/10.1080/10589759.2016.1226304.

[24] H. Sohn, C. R. Farrar, F. M. Hemez, and J. Czarnecki. *A review of structural health monitoring literature: 1996–2001*. Los Alamos National Laboratory, USA, (2003).

[25] C. Surace and R. Ruotolo. Crack detection of a beam using the wavelet transform. In *Proceedings-Spie The International Society For Optical Engineering*, (1994), pp. 1141–1147.

[26] K. M. Liew and Q. Wang. Application of wavelet theory for crack identification in structures. *Journal of Engineering Mechanics*, **124**, (2), (1998), pp. 152–157. https://doi.org/10.1061/(asce)0733-9399(1998)124:2(152).

[27] Q. Wang and X. Deng. Damage detection with spatial wavelets. *International Journal of Solids and Structures*, **36**, (23), (1999), pp. 3443–3468. https://doi.org/10.1016/s0020-7683(98)00152-8.

[28] E. Douka, S. Loutridis, and A. Trochidis. Crack identification in beams using wavelet analysis. *International Journal of Solids and Structures*, **40**, (13-14), (2003), pp. 3557–3569. https://doi.org/10.1016/s0020-7683(03)00147-1.

[29] C. C. Chang and L. W. Chen. Detection of the location and size of cracks in the multiple cracked beam by spatial wavelet based approach. *Mechanical Systems and Signal Processing*, **19**, (1), (2005), pp. 139–155. https://doi.org/10.1016/j.ymssp.2003.11.001.

[30] W. Zhang, Z. Wang, and H. Ma. Crack identification in stepped cantilever beam combining wavelet analysis with transform matrix. *Acta Mechanica Solida Sinica*, **22**, (4), (2009), pp. 360–368. https://doi.org/10.1016/s0894-9166(09)60285-8.

[31] S. Zhong and S. O. Oyadiji. Crack detection in simply supported beams without baseline modal parameters by stationary wavelet transform. *Mechanical Systems and Signal Processing*, **21**, (4), (2007), pp. 1853–1884. https://doi.org/10.1016/j.ymssp.2006.07.007.

[32] H. Gökdağ and O. Kopmaz. A new damage detection approach for beam-type structures based on the combination of continuous and discrete wavelet transforms. *Journal of Sound and Vibration*, **324**, (3-5), (2009), pp. 1158–1180. https://doi.org/10.1016/j.jsv.2009.02.030.

[33] T. V. Lien, N. T. Khiem, and T. A. Hao. Crack identification in frame structures using the stationary wavelet transform of mode shapes. *Jokull*, **64**, (6), (2014), pp. 251–262.

[34] J. C. Goswami and A. K. Chan. *Fundamentals of wavelets: theory, algorithms, and applications*. John Wiley & Sons, (2011).

[35] M. Misiti, Y. Misiti, G. Oppenheim, and J. M. Poggi. *Matlab wavelet toolbox TM 4 user's guide*. The MathWorks, Inc. Natick, Massachusetts, (2009).

[36] A. V. Ovanesova and L. E. Suarez. Applications of wavelet transforms to damage detection in frame structures. *Engineering Structures*, **26**, (1), (2004), pp. 39–49. https://doi.org/10.1016/j.engstruct.2003.08.009.

[37] X. H. Wang, R. S. H. Istepanian, and Y. H. Song. Microarray image enhancement by denoising using stationary wavelet transform. *IEEE Transactions on Nanobioscience*, **2**, (4), (2003), pp. 184–189. https://doi.org/10.1109/tnb.2003.816225.

APPENDIX 1

Frequency equation of (3) is

$$\eta^3 + a\eta^2 + b\eta + c = 0.$$

In case of $A_{12} = 0$, coefficients of above equation are

$$a = \omega^2 \left[\frac{I_{11}}{A_{33}} + \frac{I_{11}A_{22} + I_{22}A_{11}}{A_{11}A_{22}} \right], \ b = \omega^4 \left[\frac{I_{11}I_{22} - I_{12}^2}{A_{11}A_{22}} + \frac{I_{11}}{A_{33}} \frac{I_{11}A_{22} + I_{22}A_{11}}{A_{11}A_{22}} \right] - \omega^2 \frac{I_{11}}{A_{22}},$$

$$c = \omega^4 \left[\frac{\omega^2 I_{11}}{A_{33}} \frac{I_{11}I_{22} - I_{12}^2}{A_{11}A_{22}} - \frac{I_{11}^2}{A_{11}A_{22}} \right].$$

Roots of cub algebraic equation are $\eta_1(\omega), \eta_2(\omega), \eta_3(\omega)$

$$\eta_1 = -a/3 + u - b_1/u, \quad \eta_{2,3} = -a/3 - (u - b_1/u)/2 \pm i\sqrt{3}(u + b_1/u)/2,$$

where

$$u = (a_1 + \sqrt{b_1^3 + c_1^2} - a^3/27)^{1/3}, \quad a_1 = ab/6 - c/2, \quad b_1 = b/3 - a^2/9, \quad c_1 = a^3/27 - a_1.$$

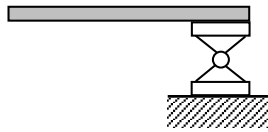Constants in formula (6) are

$$\lambda_{1,4} = \pm k_1, \quad \lambda_{2,5} = \pm k_2, \quad \lambda_{3,6} = \pm k_3, \quad k_j = \sqrt{\eta_j}, \quad j = 1, 2, 3,$$

$$\alpha_j = \frac{\omega^2 I_{12}}{\omega^2 I_{11} + \lambda_j^2 A_{11}}, \quad \beta_j = \frac{\lambda_j A_{33}}{(\omega^2 I_{11} + \lambda_j^2 A_{33})}, \quad j = 1, 2, \ldots, 6.$$
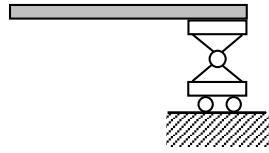
APPENDIX 2
Differential matrix operators

- Simply supported (S): $u(x,t) = M(x,t) = w(x,t) = 0$

$$[\mathbf{B}_S] = \begin{bmatrix} 1 & 0 & 0 \\ A_{12}\partial_x & A_{22}\partial_x & 0 \\ 0 & 0 & 1 \end{bmatrix}.$$

- Pined (P): $N(x,t) = M(x,t) = w(x,t) = 0$

$$[\mathbf{B}_P] = \begin{bmatrix} A_{11}\partial_x & -A_{12}\partial_x & 0 \\ A_{12}\partial_x & A_{22}\partial_x & 0 \\ 0 & 0 & 1 \end{bmatrix}.$$

- Clamped (C): $u(x,t) = \theta(x,t) = w(x,t) = 0$

$$[\mathbf{B}_C] = \begin{bmatrix} 1 & 0 & 0 \\ 0 & 1 & 0 \\ 0 & 0 & 1 \end{bmatrix}.$$

- Free (F): $N(x,t) = M(x,t) = Q(x,t) = 0$

$$[\mathbf{B}_F] = \begin{bmatrix} A_{11}\partial_x & -A_{12}\partial_x & 0 \\ A_{12}\partial_x & A_{22}\partial_x & 0 \\ 0 & -A_{33} & A_{33}\partial_x \end{bmatrix}.$$

- Simply supported beam ends (SS): $[\mathbf{B}_0] = [\mathbf{B}_L] = [\mathbf{B}_S]$.
- Pined ends (PP): $[\mathbf{B}_0] = [\mathbf{B}_L] = [\mathbf{B}_P]$.
- Simple beam (SP): $[\mathbf{B}_0] = [\mathbf{B}_S]$, $[\mathbf{B}_L] = [\mathbf{B}_P]$.
- Cantilevered beam (CF): $[\mathbf{B}_0] = [\mathbf{B}_C]$, $[\mathbf{B}_L] = [\mathbf{B}_F]$.
- Clamped beam (CC): $[\mathbf{B}_0] = [\mathbf{B}_L] = [\mathbf{B}_C]$.